Appendix 2. MT 3D Inversion Descriptions

2.1 Coso Hot Springs

From 2004 to 2011, 210 MT soundings were acquired over the Coso Hot Springs geothermal field and surrounding area in three phases (Figure 2.1.1). The purpose of conducting the MT surveys was to estimate the resistivity structure beneath the ground surface to approximately 10 km depth as could pertain to fluid flow pathways and hydrothermal alteration. The 2004 data were 101 sites collected by Quantec Geoscience Inc. under subcontract to EGI and the U.S. Navy GPO (Wannamaker et al., 2004; Newman et al., 2008) focusing on the East Flank of the CGF as part of the U.S. Dept. of Energy's Enhanced Geothermal Program research (Sheridan et al., 2003). Approximately a dozen sites were collected in 2005 at the south end of the East Flank area by Apollo Geophysics through subcontract to Lawrence Berkeley National Lab (Newman et al., 2008). The remaining ~100 sites were collected by Geosystem Inc (Western-Geco), extending the coverage to west of the Main Field (Western-Geco report to Terra-Gen Inc, 2011).

For all soundings, data were examined and those found to be of poor quality rejected. The CGF is a difficult operating environment due to strong EM noise from power plant production and a nearby interstate "DC" transmission line. The remote reference method, designed to overcome environmental noise, requires simultaneously recording sensors completely outside the influence of the noise sources. Wannamaker et al. (2004) found it necessary to use ultra-distant remote references in Parkfield CA (265 km) or Socorro, NM (1000 km). Reference sites attempted at the Centennial Flat area, 15 miles north of the CGF; Panamint Valley, 30 miles distant; and Amargosa Valley NV, 60 miles distant, were insufficiently far. The 2005 and 2011 sites did not make use of an ultra-remote reference site; the 2005 survey fortunately appeared to be conducted during a low-noise interval, but the 2011 survey was badly corrupted resulting in the rejection of large amounts of data in the 1 to 0.05 Hz, and sometimes even the 10 to 0.03 Hz, frequency range.

Data from 126 soundings at sites surrounding the main producing area were selected for inversion (Figure 2.1.1). These are primarily the recent Western-Geco sites plus a strip of sites from the East Flank area. The inversion data included at 21 frequencies from 100 Hz to 0.01 Hz. The inversion was terminated after 4 days, after 11 model updates. Calculating the predicted data and derivatives required approximately 6.75 hours for the 21 frequencies considered (approximately 20 min / frequency). Solving for the new model parameters required 46 minutes per iteration.

The resistivity structure is represented using a FE mesh consisting of 78 x 76 x 64 voxels in x (north), y (east) and z (vertical) directions (Fig. 2.1.2). The inversion domain contains 76x74 x 51 voxels leaving a rim one finite element thick around the margins of the computational model. The smallest voxels within the domain encompassed by the receivers are 120 m x 120 m wide, increasing in width towards the periphery of the FE mesh.

The FE mesh was deformed such that the nodes at the air/earth interface follow the topography, generated from ASTER GDEM data downloaded from http://gdex.cr.usgs.gov/gdex/. The ASTER GDEM is a product of METI and NASA, courtesy of

the online Data Pool at the NASA Land Processes Distributed Active Archive Center (LP DAAC), USGS/Earth Resources Observation and Science (EROS) Center, Sioux Falls, South Dakota (https://lpdaac.usgs.gov/data_access). Topographic relief is concentrated along the margins of the survey area; a surface elevation of 1230 m was assigned to the background layered model. Background layer thicknesses and minimum and maximum deformation of the inversion voxels are listed in Table 2.1.1. The starting model, also used as the a-priori constraint, consists of a 27 Ωm halfspace, estimated from the frequency-weighted average of the xy and yx mode apparent resistivity data.

Convergence is shown in Figure 2.1.3, with nRMS decreasing from 11.1 for the starting model (#1) to 3.84 for model 9. Model 9 was chosen to represent the subsurface resistivity structure as subsequent models did not have significantly lower nRMS despite substantially decreasing the applied regularization, suggesting that the inversion has reached a minimum. A map color-coded according to the final nRMS for each MT station is provided in Fig. 2.1.4. The extremely poor misfit affecting stations such as CosoE38 is attributed primarily to the inclusion of poor quality data which were not caught prior to the inversion (Fig. 2.1.5). In the case of COSOE38, the first 3 Kzy data have unreasonably large magnitudes (shown as out-of-bounds); their misfit inflating the sounding nRMS. In addition, there is systemic misfit of a cross-over in the observed Zyy data at mid-range frequencies at several stations. We hypothesize that this is due to over-regularization in part of the inversion domain, restricting and possibly suppressing developing structures. Further investigations of this are planned.

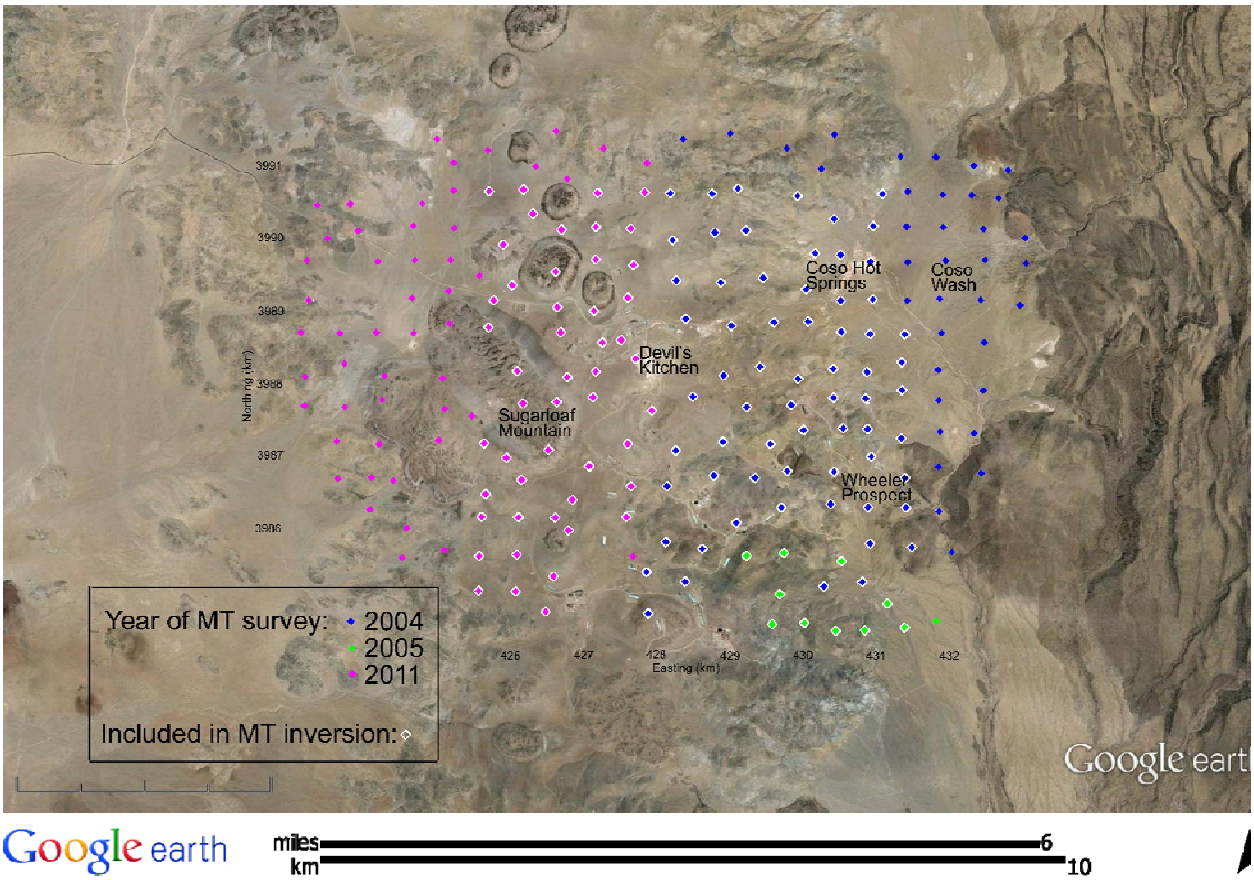

Figure 2.1.1. Google earth map of the Coso Hot Springs geothermal field with the MT stations collected in 2004, 2005 and 2011 coded by color (blue, green, pink).

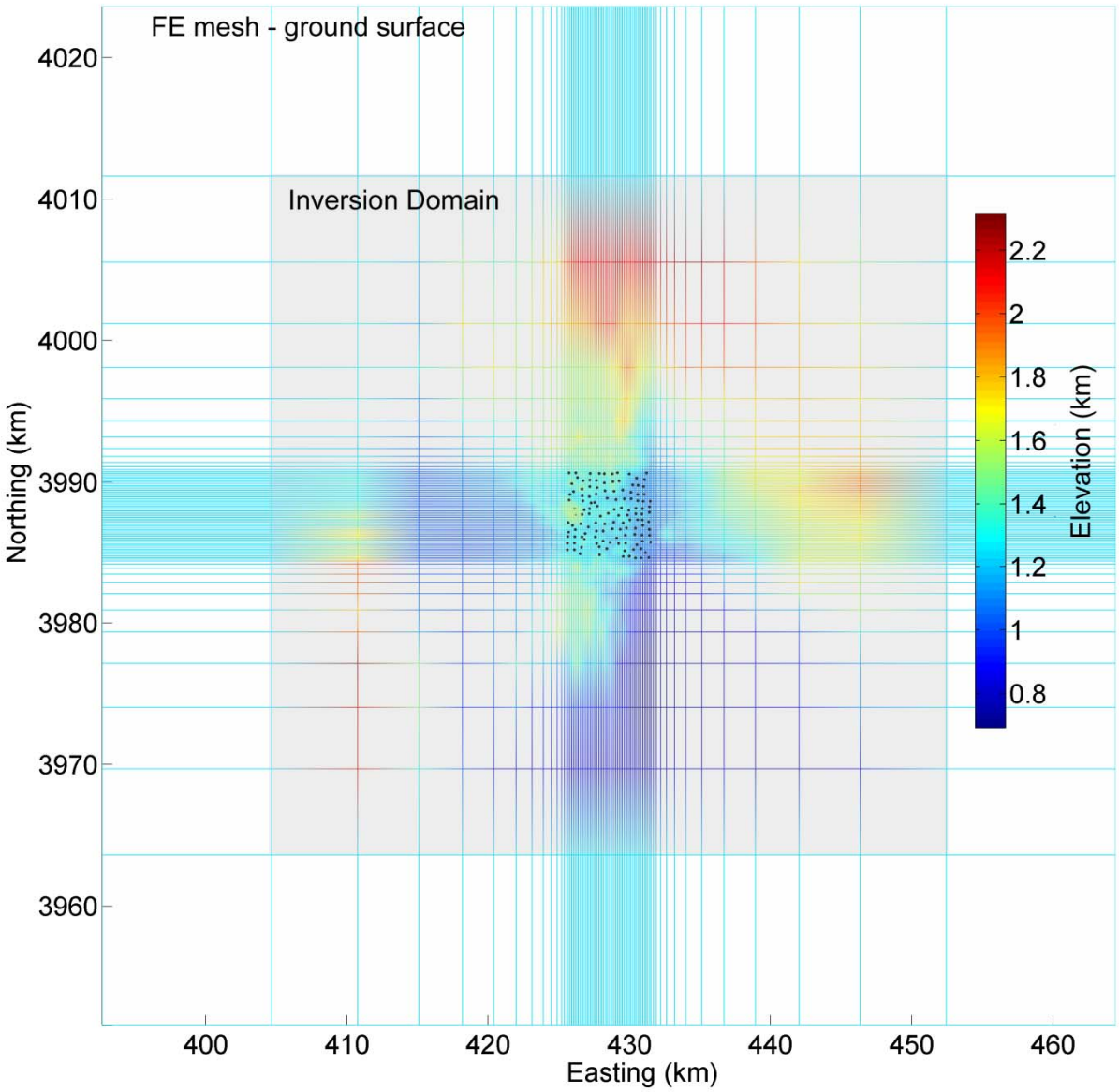

Figure 2.1.2. FE mesh

Table 2.1.1 Description of the horizontal background layers, and voxel deformation beneath the ground surface.

Elevation (km asl) of background layer top	Background layer thickness (km)	Minimum thickness of deformed voxel (km)	Maximum thickness of deformed voxel (km)	Inversion layer
1.23	0.06	0.06	0.06	1
1.17	0.065	0.094038	0.050618	2
1.105	0.07	0.101272	0.054512	3
1.035	0.075	0.108505	0.058406	4
0.96	0.08	0.115739	0.0623	5
0.88	0.085	0.122973	0.066193	6
0.795	0.09	0.130206	0.070087	7
0.705	0.095	0.13744	0.073981	8
0.61	0.1	0.144674	0.077874	9
0.51	0.105	0.151907	0.081768	10
0.405	0.11	0.159141	0.085662	11
0.295	0.115	0.166375	0.089556	12
0.18	0.12	0.173608	0.093449	13
0.06	0.13	0.188076	0.101237	14
-0.07	0.14	0.202543	0.109024	15
-0.21	0.15	0.21701	0.116812	16
-0.36	0.16	0.231478	0.124599	17
-0.52	0.17	0.245945	0.132386	18
-0.69	0.18	0.260413	0.140174	19
-0.87	0.19	0.27488	0.147961	20
-1.06	0.2	0.289347	0.155749	21
-1.26	0.21	0.21	0.21	22
-1.47	0.22	0.22	0.22	23
-1.69	0.23	0.23	0.23	24
-1.92	0.24	0.24	0.24	25
-2.16	0.25	0.25	0.25	26
-2.41	0.26	0.26	0.26	27
-2.67	0.27	0.27	0.27	28
-2.94	0.28	0.28	0.28	29
-3.22	0.29	0.29	0.29	30
-3.51	0.3	0.3	0.3	31
-3.81	0.32	0.32	0.32	32
-4.13	0.34	0.34	0.34	33
-4.47	0.36	0.36	0.36	34
-4.83	0.38	0.38	0.38	35
-5.21	0.4	0.4	0.4	36
-5.61	0.42	0.42	0.42	37

-6.03	0.44	0.44	0.44	38
-6.47	0.47	0.47	0.47	39
-6.94	0.51	0.51	0.51	40
-7.45	0.55	0.55	0.55	41
-8	0.6	0.6	0.6	42
-8.6	0.66	0.66	0.66	43
-9.26	0.73	0.73	0.73	44
-9.99	0.8	0.8	0.8	45
-10.79	0.9	0.9	0.9	46
-11.69	1	1	1	47
-12.69	1.2	1.2	1.2	48
-13.89	1.5	1.5	1.5	49
-15.39	1.8	1.8	1.8	50
-17.19	2	2	2	51
-19.19	4	4	4	Fixed
-23.19	8	8	8	Fixed
-31.19	16	16	16	Fixed
-47.19				

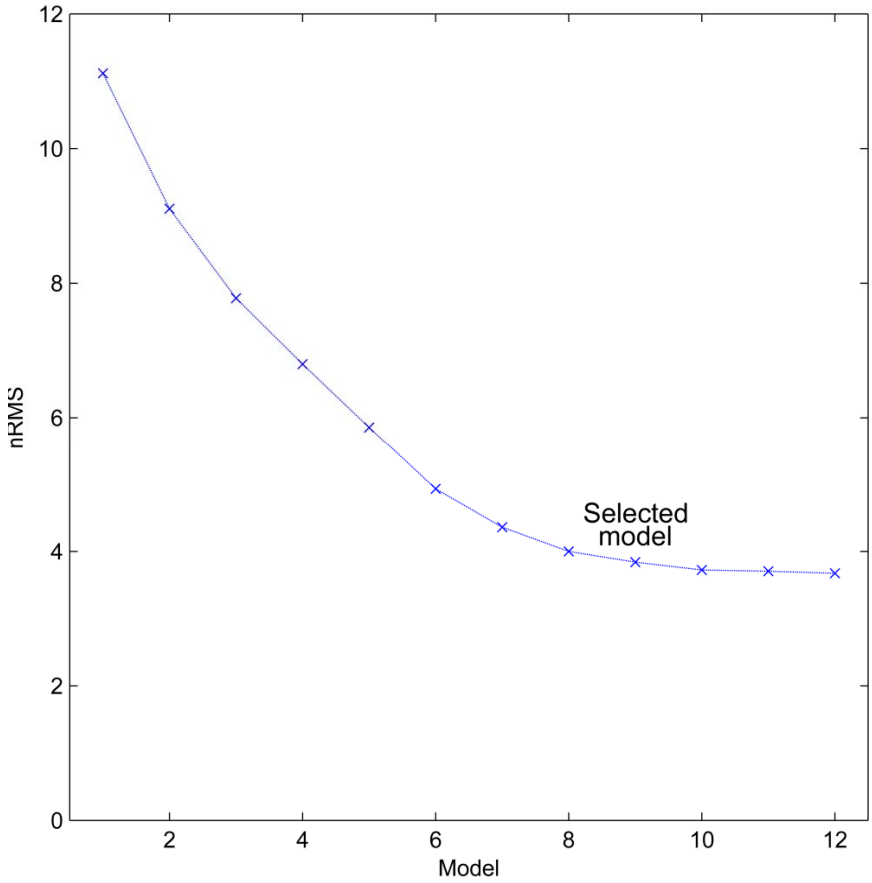

Figure 2.1.3. nRMS calculated using the data predicted at each subsequent model. The starting model is #1.

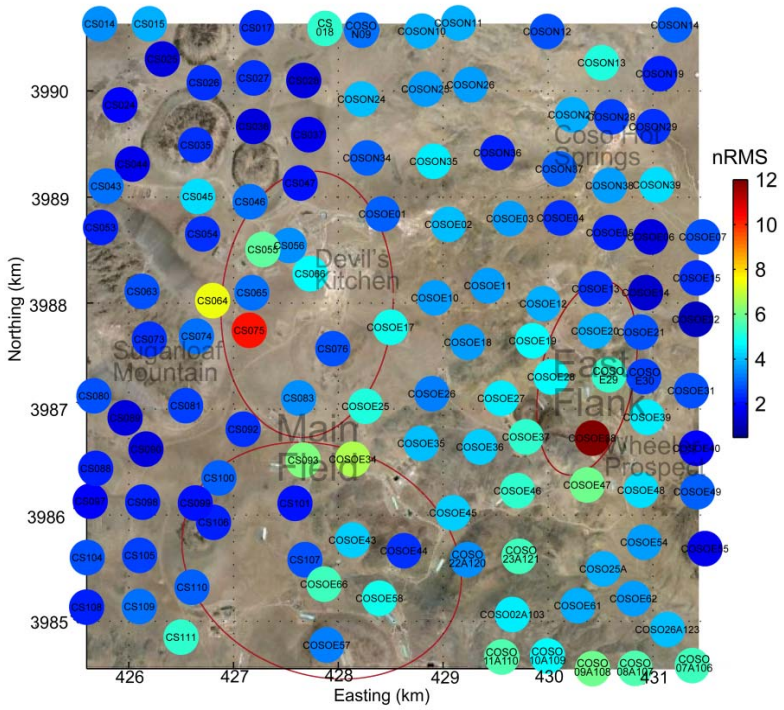

Figure 2.1.4. nRMS at each receiver, overlaid on the Google earth image of the area.

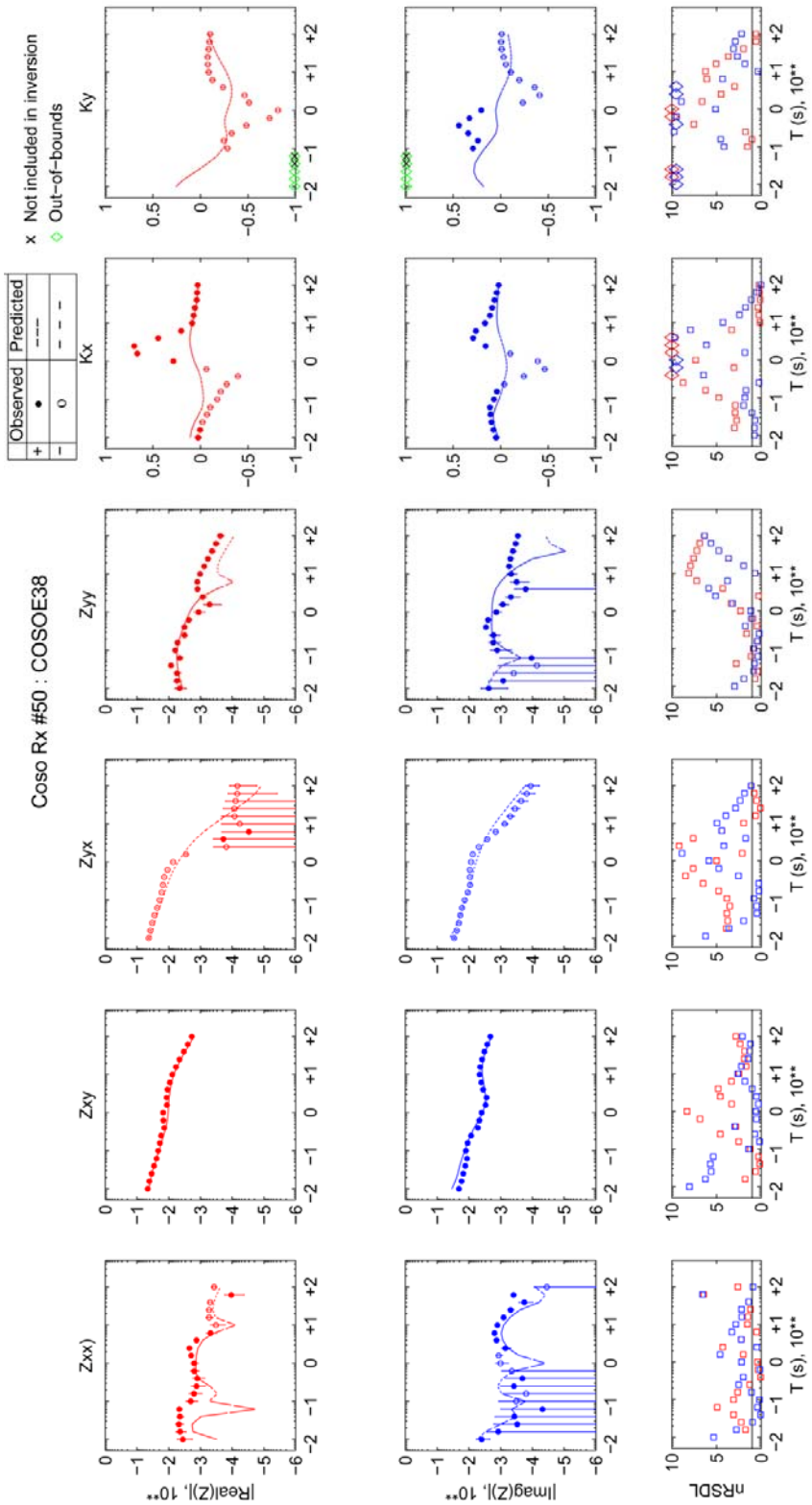

Figure 2.1.5. Sounding COSOE38.

2.2 Lightning Dock

In 2010, Quantec Geoscience Inc collected 42 MT soundings, on average ~2 km apart, spanning a frequency range of 320 Hz to 0.001 Hz (Fig. 2.2.1). An additional 18 soundings, spaced approximately 700 m apart, were collected in 2014.

The resistivity structure is represented using a finite element (FE) mesh embedded in a horizontally 1D background. The FE mesh consists of 88 x 98x 54 voxels in x (north), y (east) and z (vertical) directions (Fig 2.2.2). There are 10 z-layers of voxels above the ground surface (air). 84 x 94 x 41 voxels are inversion parameters. MT stations as modeled in the program may be laterally offset from their true location in order to accommodate the program requirement that the station be horizontally centered on a voxel.

Voxels within the domain encompassed by the receivers have lateral dimensions of 150 m x 150. The FE mesh is deformed vertically to represent topography, using a digital elevation model down-loaded from the US Geological Survey website, http://gdex.cr.usgs.gov/gdex/. Topographic relief (< 700 m) is concentrated along the margins of the survey area; most MT receivers have elevations close to 1250 m (Figure 2.2.2). Background layer thicknesses and minimum and maximum deformation of the inversion voxels are listed in Table 2.2.1. These background layer thicknesses represent the nominal voxel thicknesses before deforming them vertically to accommodate the surface topography. The starting model, also used as the a-priori constraint, was determined by 1D inversion of a sounding derived from the average of the off-diagonal impedances (a rotational invariant) over all frequencies.

Data from all 60 soundings were included in the inversion, at 25 frequencies (7 per decade) ranging from 100 Hz to 0.025 Hz. The inversion was terminated after 4 days, having completed 12 model updates. Calculating the predicted data and derivatives required approximately 7 hours and 10 minutes (approximately 17 min / frequency). Solving for the new model parameters required 28 minutes per iteration.

Convergence is shown in Figure 2.2.3, with nRMS decreasing from from 6.15 for the starting model (#1) to 0.95 for model #12. The data are largely fit by model 7 (nRMS=1.1). Subsequent models demonstrate better fit to the data, but are calculated with reduced enforcement of spatial smoothness. Model 9 may be a good compromise between the two. A map color-coded according to the model 9 nRMS for each MT station is provided in Fig. 2.2.4.

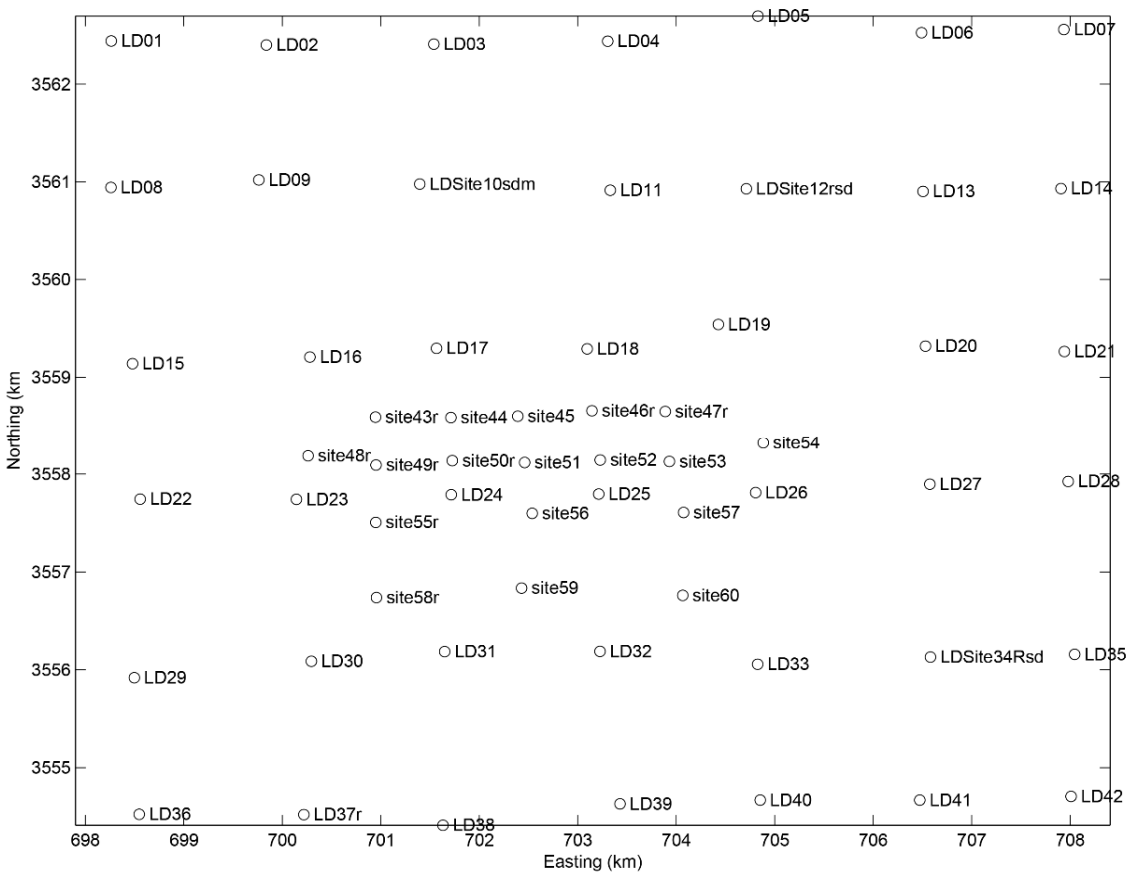

Figure 2.2.1. Survey Geometry. Data at stations labeles as LDxx were collected in 2010; Data at stations labeled as sitexx were collected in 2014.

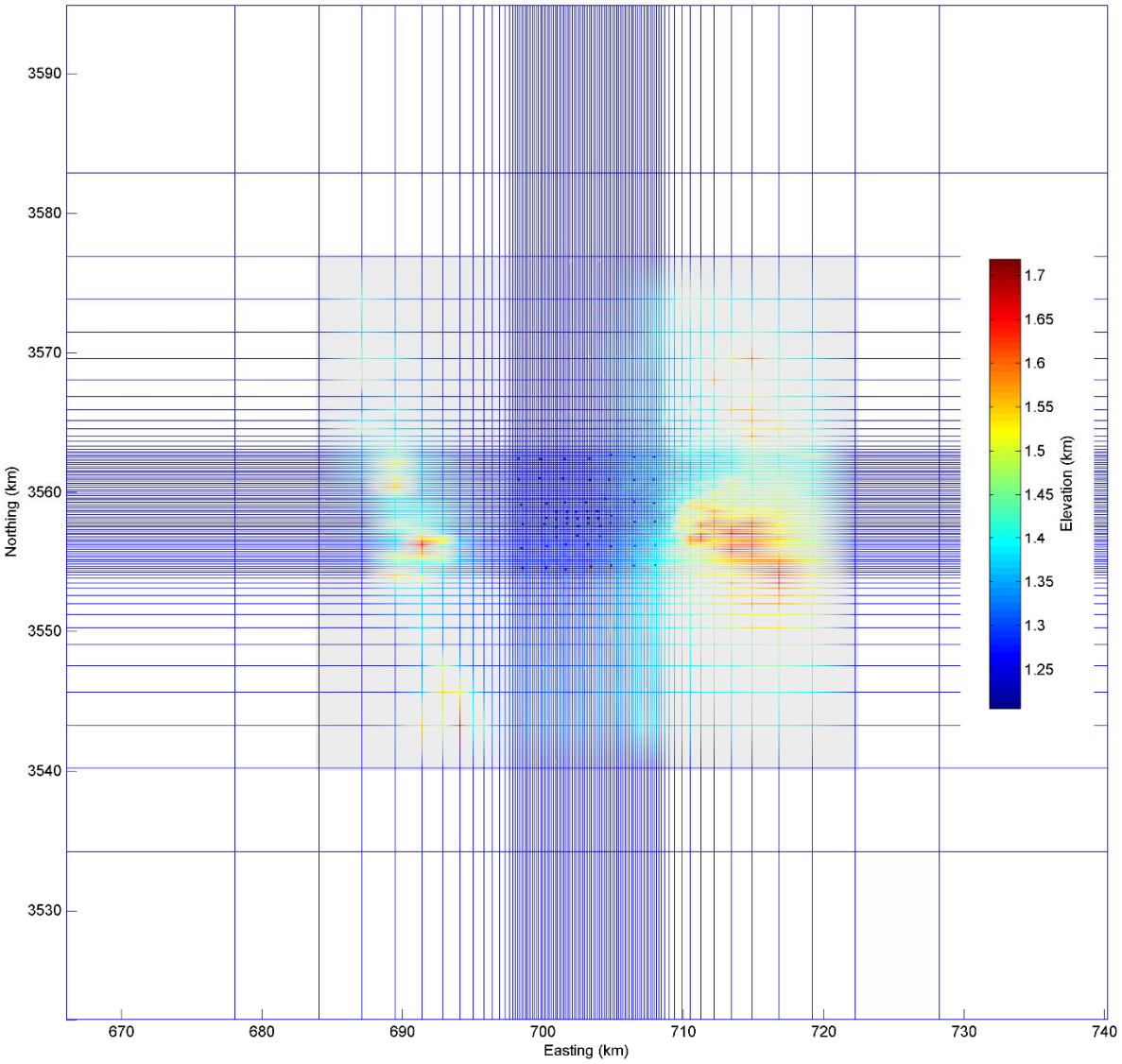

Figure 2.2.2. Horizontal distribution of the FE mesh and interpolated ground surface elevation. The gray area denotes FE voxels which are part of the inversion domain. Receiver locations are indicated by dots.

Table 2.2.1. Description of the horizontally layered background and vertical mesh description.

Elevation (km asl) of background layer top	Background layer thickness (km)	Max thickness of deformed voxel (km)	Min thickness of deformed voxel (km)	Start & a-priori model resistivity (ohm.m)	Lateral Model Weights
1.25	0.125	0.125	0.125	16.2	200
1.125	0.125	0.134	0.124	14.1	100
1.0	0.13	0.139	0.129	16.2	50
0.87	0.14	0.150	0.139	15.8	25
0.73	0.15	0.161	0.149	15.4	12.5
0.58	0.16	0.172	0.159	15.8	6.25
0.42	0.17	0.182	0.169	16.9	3.125
0.24	0.18	0.193	0.179	18.9	1.5625
0.07	0.19	0.204	0.189	21.6	1
-0.12	0.2	0.215	0.199	25.0	1
-0.32	0.21	0.225	0.209	29.6	1
-0.53	0.22	0.236	0.218	35.4	1
-0.75	0.23	0.247	0.228	42.8	1
-0.98	0.24	0.257	0.238	51.8	1
-1.22	0.25	0.268	0.248	62.8	1
-1.47	0.26	0.279	0.258	76.1	1
-1.73	0.27	0.290	0.268	90.9	1
-2.0	0.28	0.300	0.278	105.1	1
-2.28	0.29	0.311	0.288	118.6	1
-2.57	0.3	0.322	0.298	129.9	1
-2.87	0.31	0.333	0.308	137.3	1
-3.18	0.32	0.313	0.318	139.9	1
-3.5	0.33	0.354	0.328	137.7	1
-3.83	0.34	0.365	0.338	143.5	1
-4.17	0.36	0.386	0.357	148.7	1
-4.52	0.38	0.408	0.377	146.9	1
-4.91	0.40	0.429	0.397	138.9	1
-5.31	0.42	0.42	0.42	126.8	1
-5.73	0.44	0.44	0.44	113.1	1
-6.17	0.47	0.47	0.47	98.2	1
-6.64	0.51	0.51	0.51	88.7	1
-7.15	0.55	0.55	0.55	80.9	1
-7.7	0.6	0.6	0.6	71.9	1
-8.3	0.66	0.66	0.66	64.3	1
-8.96	0.72	0.72	0.72	57.2	1
-9.68	0.88	0.88	0.88	52.7	1
-10.56	1.1	1.1	1.1	50.8	1
-11.66	1.30	1.30	1.30	45.8	1
-12.96	1.8	1.8	1.8	42.2	1
-14.76	2.49	2.49	2.49	44.2	1
-17.25	3.50	3.50	3.50	45.1	1
-20.75	7.0	7.0	7.0	45.9	1
-27.75	14.0	14.0	14.0	53.1	1
-41.75	28.0	28.0	28.0	50.0	1
-69.75 (bottom)					

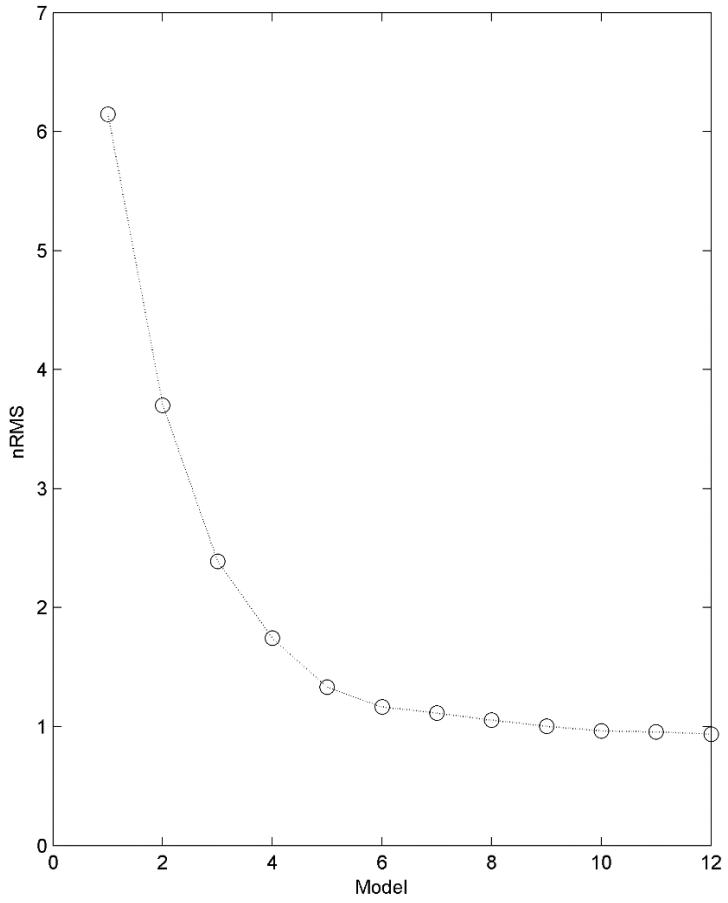

Figure 2.2.3. Convergence of the 3D inversion.

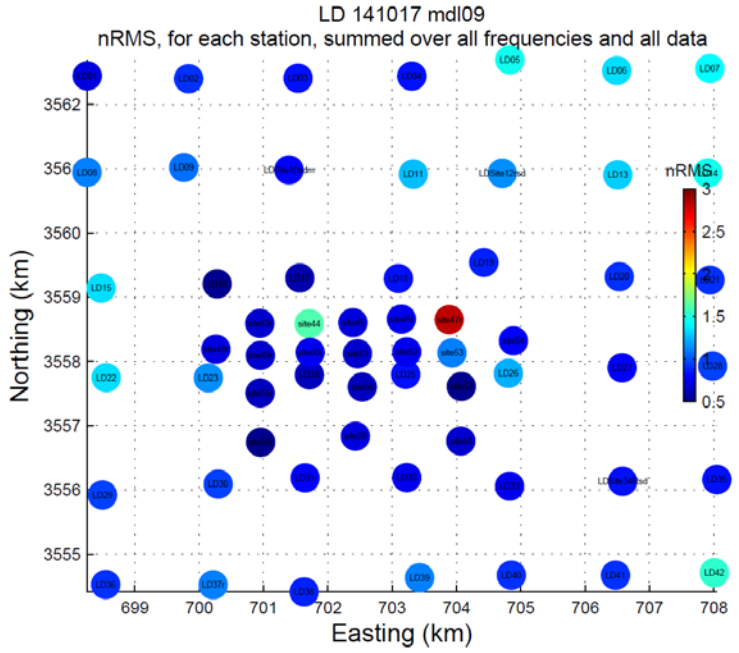

Fig. 2.2.4. Distribution of the misfit.

2.3 Thermo Hot Springs

Data from 90 MT soundings were provided by Cyrq Energy for this project. The locations of the survey sites are shown in (Fig. 2.3.1). The resistivity structure is represented using a FE mesh consisting of 93 x 98 x 65 voxels in x (north), y (east) and z (vertical) directions (Fig 2.3.2). There are 89 x 94 x 52 inversion parameters. Voxels within the domain encompassed by the receivers are 400 m x 400 m wide, increasing in width towards the periphery of the FE mesh.

The FE mesh was deformed such that the nodes at the air/earth interface follow the topography, generated from ASTER GDEM data downloaded from http://gdex.cr.usgs.gov/gdex/. The ASTER GDEM is a product of METI and NASA, courtesy of the online Data Pool at the NASA Land Processes Distributed Active Archive Center (LP DAAC), USGS/Earth Resources Observation and Science (EROS) Center, Sioux Falls, South Dakota (https://lpdaac.usgs.gov/data_access). Topographic relief (< 1500 m) is concentrated along the margins of the survey area; a surface elevation of 1600 m was assigned to the background layered model (Figure 2.3.2). Background layer thicknesses and minimum and maximum deformation of the inversion voxels are listed in Table 2.3.1.

Data from all 90 soundings were included in the inversion, at 16 frequencies (4 per decade) ranging from 180 Hz to 0.032 Hz. By trial and error, it was found that setting the minimum floor applied to the model weights to 10% of the maximum model weight and the regularization multiplier to scale proportionately to the nRMS yielded a suitable model, fitting the data while minimizing roughness. The inversion was terminated after 5 days, having completed 10 model updates (Figure 2.3.3). Within this time, an additional 2 model updates were completed but were rejected because they did not sufficiently improve the nRMS of the predicted data with respect to that of the previous model. When this occurs, the inversion re-calculates the model using a reduced regularization penalty. Calculating the predicted data and derivatives required approximately 8 hours for the 16 frequencies considered (approximately 30 min / frequency). Solving for the new model parameters required 50 minutes per iteration.

Convergence is shown in Figure 2.3.3, with nRMS decreasing from 9.75 for the starting model (#1) to 1.16 for model #11. The inversion was stopped after the predicted data for model #11 was calculated; it was judged that the nRMS was sufficiently small and likely to improve only marginally with subsequent iterations. There is however a systematic larger misfit in the Zxx mode, most evident for stations 45, 69, 70, 71 and 72 and affecting those stations immediately to the east (Fig. 2.3.4).

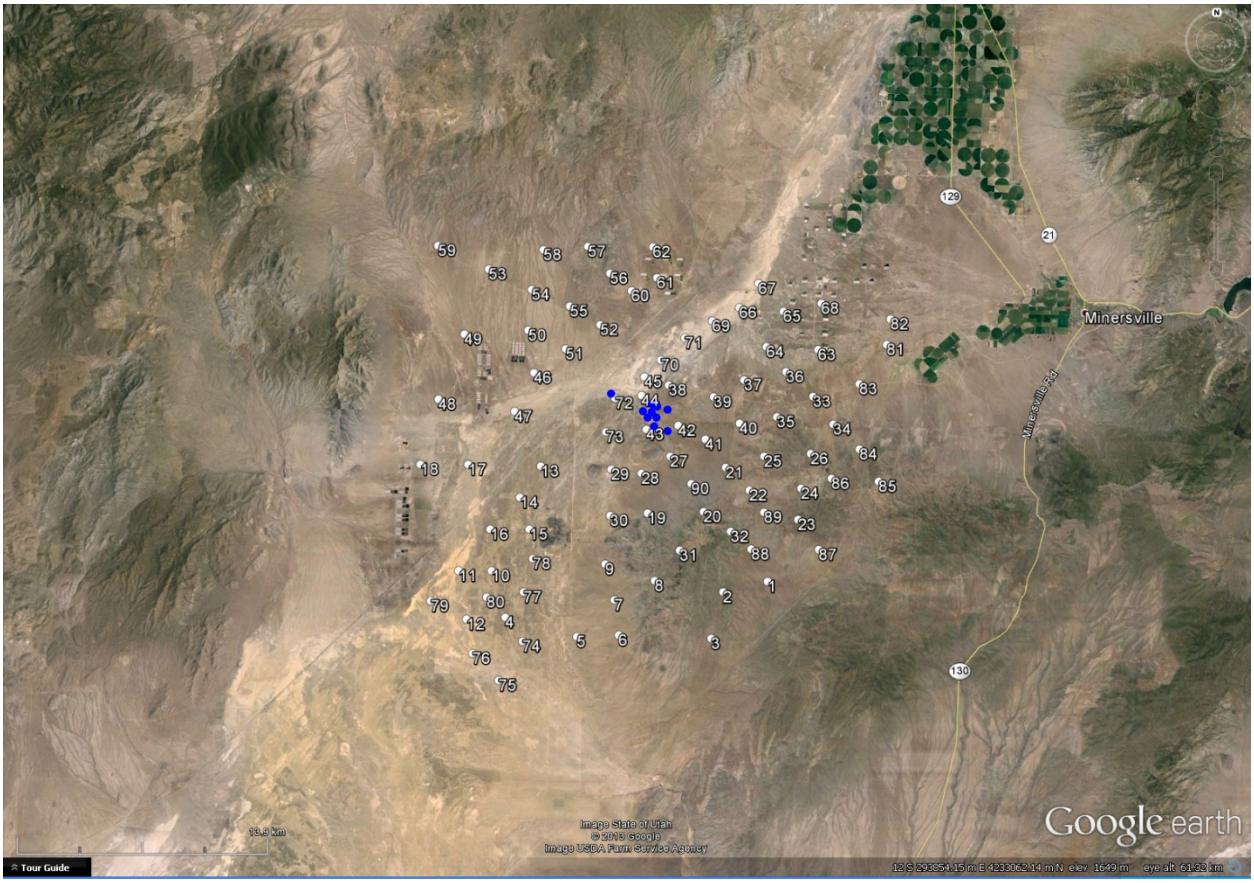

Figure 2.3.1. Map of the survey area showing the MT station locations 1 to 90, and geothermal wells (blue dots).

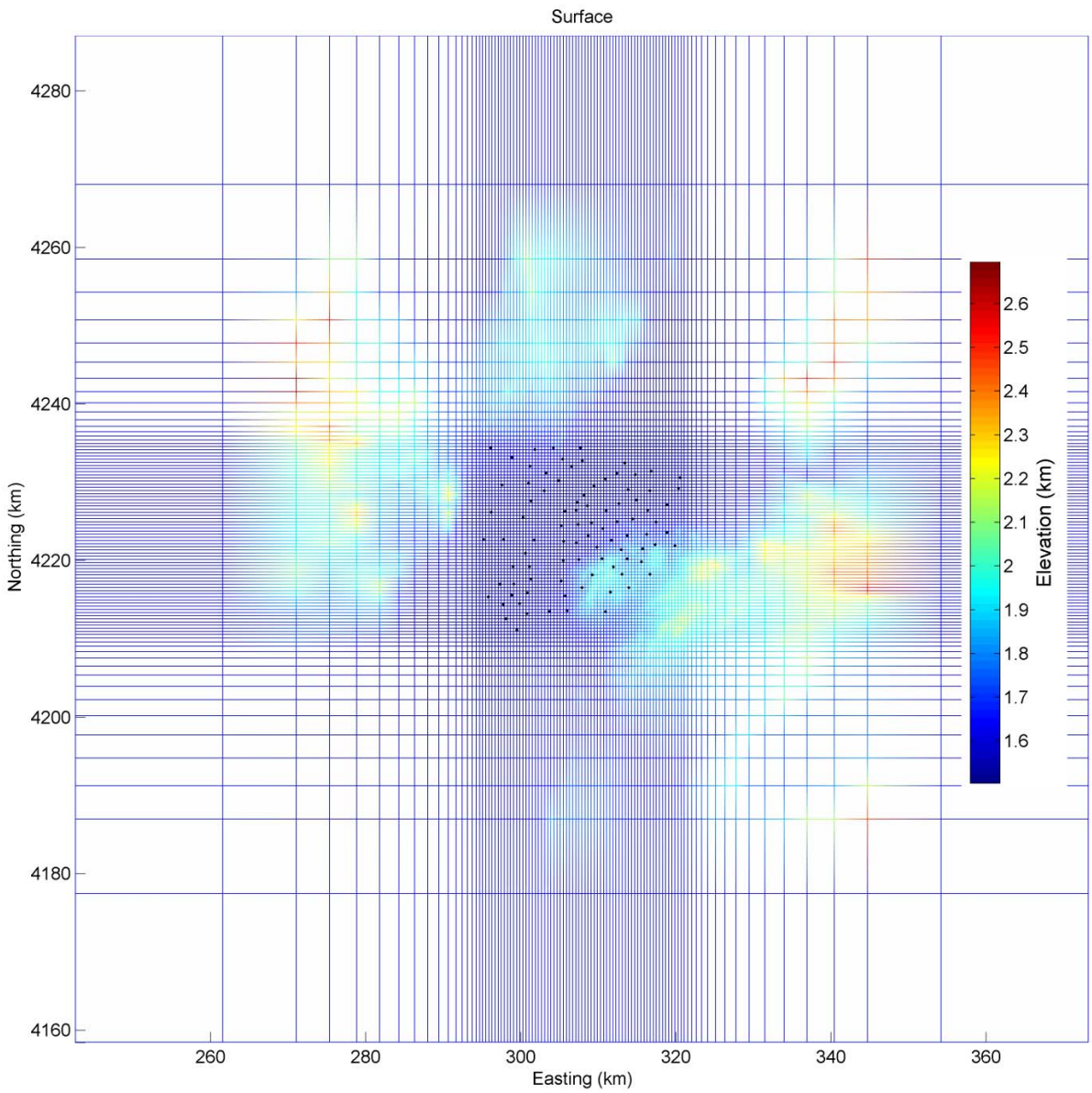

Figure 2.3.2. Horizontal distribution of the FE mesh and interpolated ground surface elevation. The gray area denotes FE voxels which are part of the inversion domain. Receiver locations are indicated by black dots.

Table 2.3.1. Description of the horizontally layered background and vertical mesh.

Elevation (km asl) of background layer top	Background layer thickness (km)	Minimum thickness of deformed voxel (km)	Maximum thickness of deformed voxel (km)	Start & a-priori model resistivity (Ωm)
1.600	0.08	0.08	0.08	50.0
1.520	0.085	0.1188	0.082	50.0
1.435	0.09	0.1258	0.0868	48.92
1.345	0.095	0.1327	0.0917	44.40
1.250	0.1	0.1397	0.0965	27.55
1.150	0.105	0.1467	0.1013	20.98
1.045	0.11	0.1537	0.1061	21.83
0.935	0.115	0.1607	0.111	24.70
0.820	0.12	0.1677	0.1158	35.69
0.700	0.125	0.1747	0.1206	40.96
0.575	0.13	0.1816	0.1254	51.51
0.445	0.135	0.1886	0.1303	64.99
0.310	0.14	0.1956	0.1351	79.89
0.170	0.145	0.2026	0.1399	95.44
0.025	0.15	0.2096	0.1447	111.2
-0.125	0.16	0.2236	0.1544	129.1
-0.285	0.17	0.2375	0.164	147.8
-0.455	0.18	0.2515	0.1737	167.0
-0.635	0.19	0.2655	0.1833	186.4
-0.825	0.2	0.2794	0.193	205.8
-1.025	0.21	0.2934	0.2026	225.0
-1.235	0.22	0.22	0.22	243.7
-1.455	0.23	0.23	0.23	261.8
-1.685	0.24	0.24	0.24	279.1
-1.925	0.25	0.25	0.25	295.5
-2.175	0.26	0.26	0.26	310.9
-2.435	0.27	0.27	0.27	325.1
-2.705	0.28	0.28	0.28	338.0
-2.985	0.29	0.29	0.29	349.7
-3.275	0.3	0.3	0.3	360.0
-3.575	0.32	0.32	0.32	376.9
-3.895	0.34	0.34	0.34	392.1
-4.235	0.36	0.36	0.36	405.5
-4.595	0.38	0.38	0.38	416.0
-4.975	0.4	0.4	0.4	426.1
-5.375	0.42	0.42	0.42	433.0
-5.795	0.44	0.44	0.44	437.7
-6.235	0.47	0.47	0.47	446.5
-6.705	0.51	0.51	0.51	458.2
-7.215	0.55	0.55	0.55	465.7
-7.765	0.6	0.6	0.6	474.2
-8.365	0.66	0.66	0.66	482.3
-9.025	0.73	0.73	0.73	488.3
-9.755	0.8	0.8	0.8	486.3
-10.555	0.9	0.9	0.9	487.7
-11.455	1	1	1	479.8
-12.455	1.12	1.12	1.12	467.4
-13.575	1.25	1.25	1.25	446.3
-14.825	1.5	1.5	1.5	436.1
-16.325	1.85	1.85	1.85	546.1
-18.175	2.2	2.2	2.2	500
-20.375	2.7	2.7	2.7	500
-23.075	5.4	5.4	5.4	100
-28.475	10.8	10.8	10.8	35.64
-39.275	21.60	21.6	21.6	50 (halfspace)
(-60.875 bottom)				

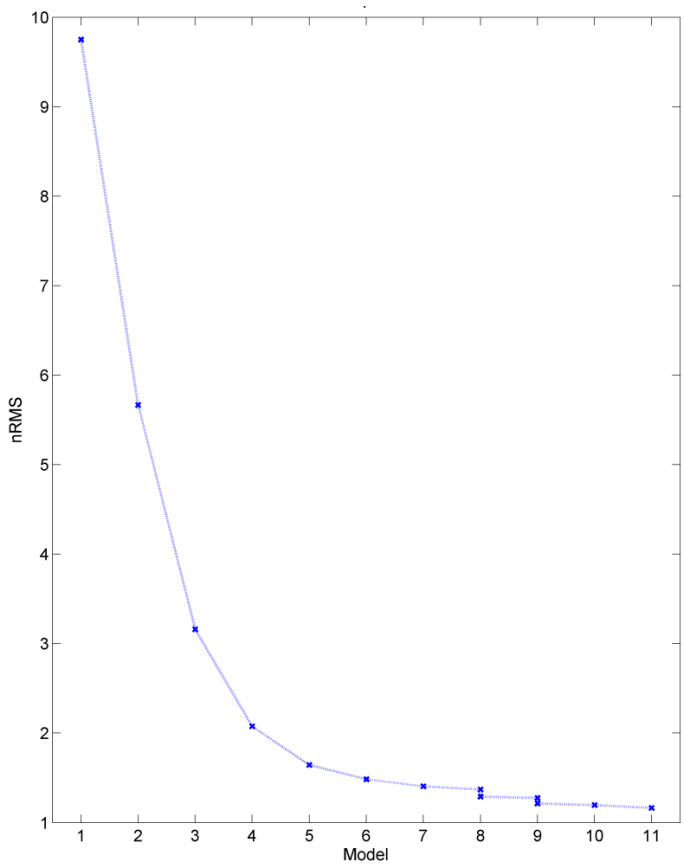

Figure 2.3.3. Convergence of the 3D inversion. Note that initially calculated models 8 and 9 had less than 5% reduction in predicted data nRMS with respect to that of the previous model. In these instances, the regularization multiplier is halved and the model is re-calculated prior to continuing the inversion process, provided that the 5% reduction criteria is now met.

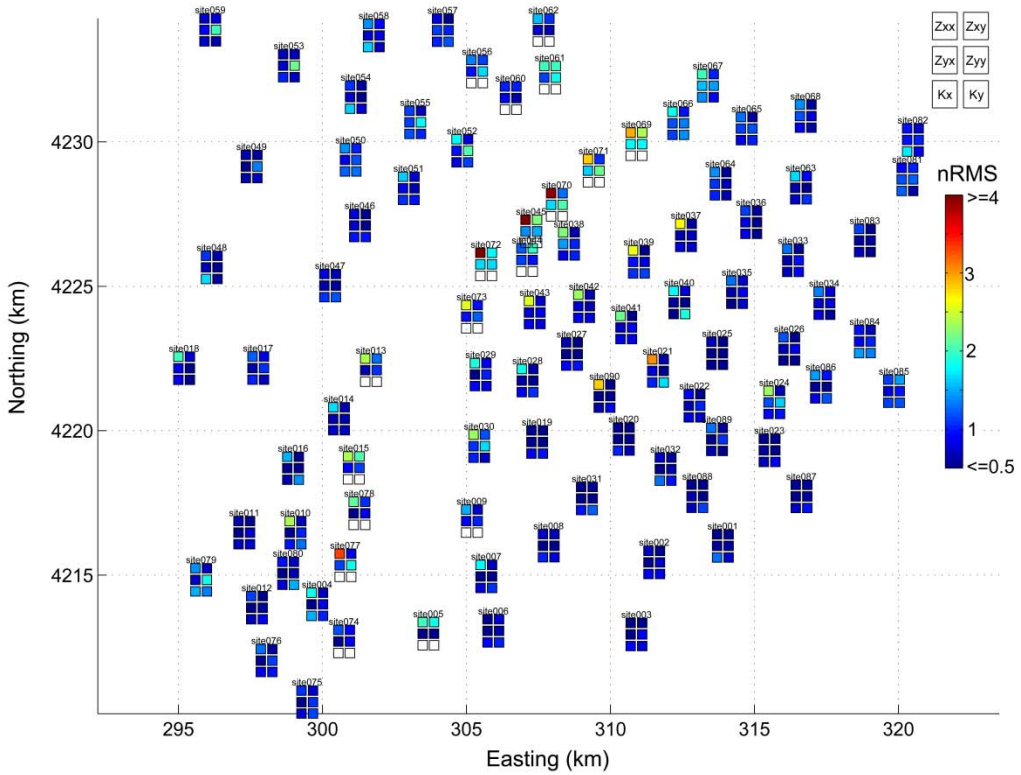

Figure 2.3.4. nRMS for each station, separated by mode.

2.4 Raft River

In 2011, 105 MT soundings spaced 0.5 to 1 km apart were collected over the Raft River geothermal system, with the highest density near the well field (Fig. 2.4.1). The resistivity structure is represented using a FE mesh consisting of 93 x 94 x 63 voxels in x (north), y (east) and z (vertical) directions (Fig. 2.4.2). The FE mesh was deformed such that the nodes at the air/earth interface follow the topography, generated from ASTER GDEM data downloaded from http://gdex.cr.usgs.gov/gdex/. The ASTER GDEM is a product of METI and NASA, courtesy of the online Data Pool at the NASA Land Processes Distributed Active Archive Center (LP DAAC), USGS/Earth Resources Observation and Science (EROS) Center, Sioux Falls, South Dakota (https://lpdaac.usgs.gov/data_access).

The inversion domain contains 89 x 90 x 49 voxels. The smallest voxels within the domain encompassed by the receivers are 100 m x 100 m wide, increasing in width towards the periphery of the FE mesh. Topographic relief is concentrated along the margins of the survey area; a surface elevation of 1500 m was assigned to the background layered model (Fig. 2.4.2). Background layer thicknesses and minimum and maximum deformation of the inversion voxels are listed in Table 2.4.1. A graphic representation of the background resistivity distribution is provided in Fig. 2.4.3.

Data from all 105 soundings were included in the inversion, at 24 frequencies from 100 Hz to 0.0375 Hz. The inversion was stopped after 11 model updates. Calculating the predicted data and derivatives required approximately 13 hours for the 24 frequencies considered (approximately 28 min / frequency). Solving for the new model parameters required approximately 75 minutes per iteration.

Convergence is shown in Figure 2.4.4, with nRMS decreasing from 6.38 for the starting model (#1) to 1.28 for model 12. A map color-coded according to the final nRMS for each MT station is provided in Fig. 2.4.5. The data is essentially well-fit over the survey area for the given data weights, with the exception of site RR-20, which suffers from poorly fit tipper data dissimilar to that of the surrounding stations.

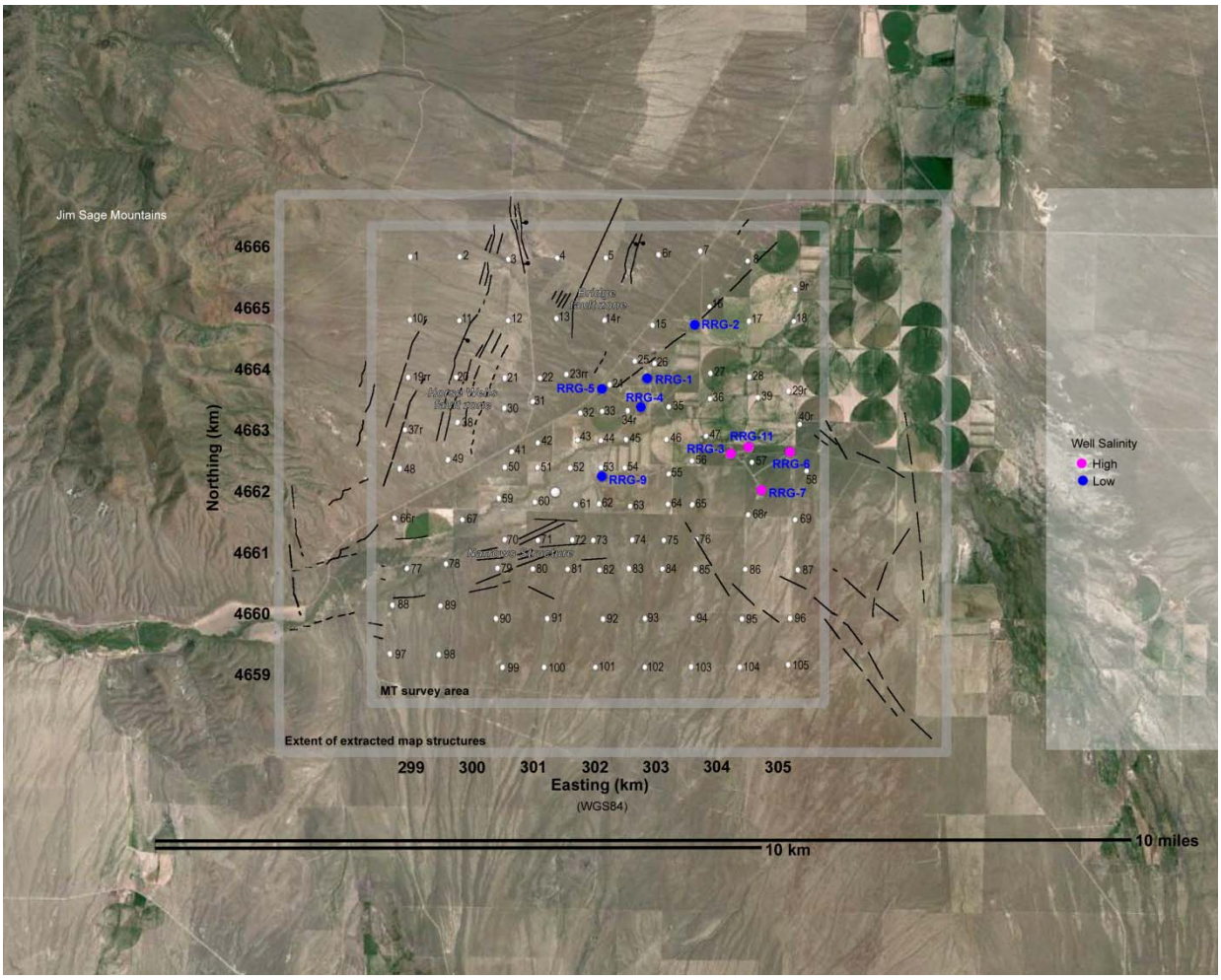

Figure 2.4.1. MT sounding locations, geothermal wells, colored according to whether they contain high or low salinity deep geothermal fluids (Ayling and Moore, 2013), and mapped faults.

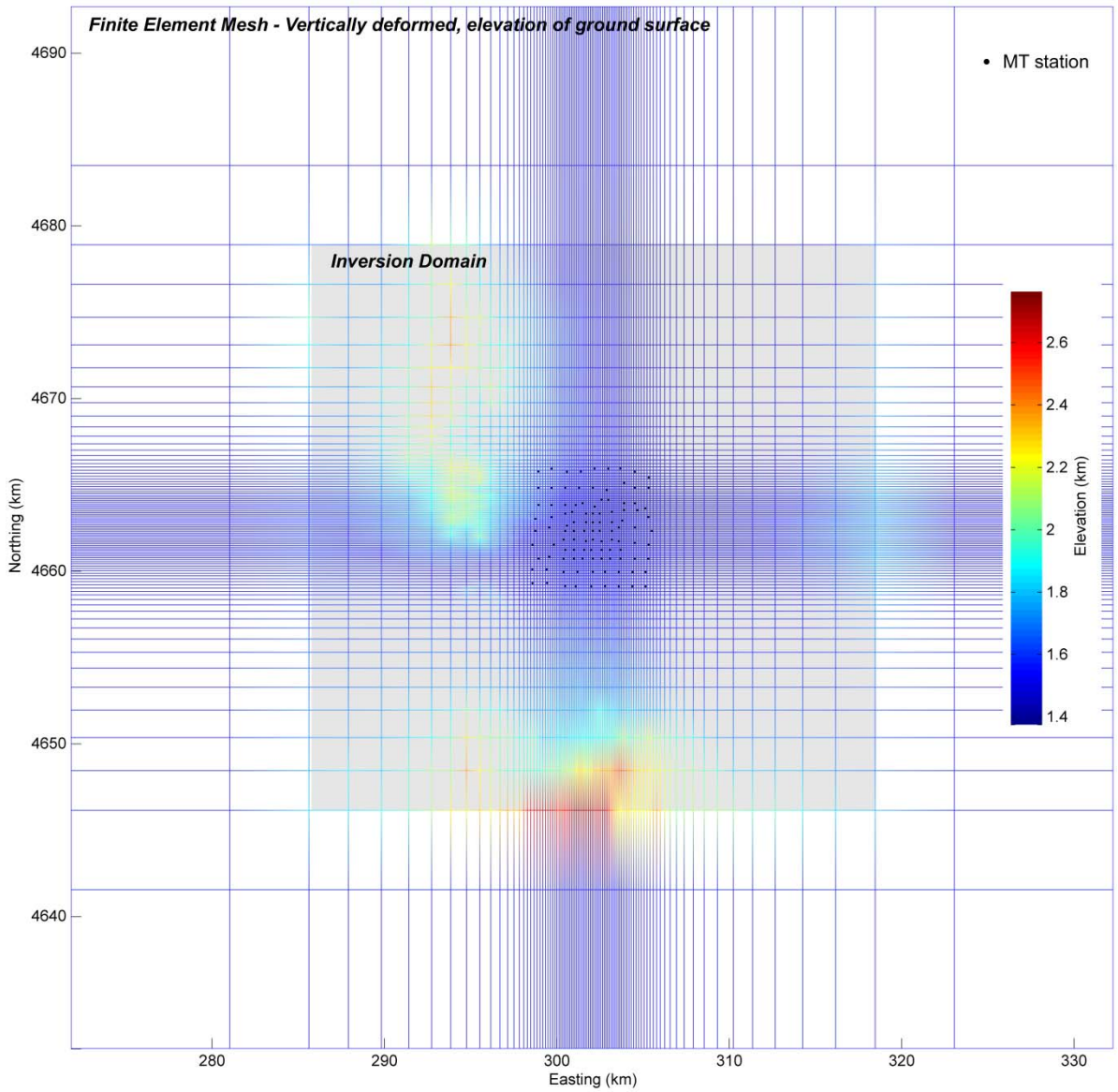

Figure 2.4.2. Plan view of the finite-element mesh used to model the MT data, with interpolated ground-surface elevations at each node and receiver locations (black dots). The inversion domain is the shaded area.

Table 2.4.1. Description of the horizontal background layers, starting and a-priori resistivity structure, and voxel deformation beneath the ground surface.

Elevation (km asl) of background layer top	Background layer thickness (km)	Minimum thickness of deformed voxel (km)	Maximum thickness of deformed voxel (km)	Start & a-priori model resistivity (ohm.m)	Horizontal Weights
1.500	0.060	0.060	0.060	13.5318	1200
1.440	0.065	0.086	0.063	8.7032	600
1.375	0.070	0.093	0.068	8.0775	300
1.305	0.075	0.010	0.072	9.4073	150
1.230	0.080	0.106	0.077	8.4674	75
1.150	0.085	0.113	0.082	6.0024	37.5
1.065	0.090	0.120	0.087	6.1843	25
0.975	0.095	0.126	0.092	9.7656	12.5
0.880	0.100	0.133	0.097	13.7552	6.25
0.780	0.105	0.139	0.102	17.762	3.125
0.675	0.110	0.146	0.106	21.692	1.5625
0.565	0.115	0.153	0.111	25.4453	1
0.450	0.12	0.159	0.116	28.8184	1
0.330	0.13	0.173	0.126	33.4448	1
0.200	0.14	0.186	0.135	39.6825	1
0.060	0.15	0.199	0.145	43.8596	1
-0.090	0.16	0.213	0.155	44.4444	1
-0.250	0.17	0.226	0.164	43.29	1
-0.420	0.18	0.239	0.174	42.0168	1
-0.600	0.19	0.252	0.184	41.6667	1
-0.790	0.20	0.266	0.193	42.3729	1
-0.990	0.21	0.279	0.203	44.4444	1
-1.200	0.22	0.292	0.213	46.9484	1
-1.420	0.23	0.306	0.222	45.2489	1
-1.650	0.24	0.319	0.232	35.8423	1
-1.890	0.25	0.332	0.242	37.1747	1
-2.140	0.26	0.345	0.252	34.7222	1
-2.400	0.27	0.27	0.27	29.1545	1
-2.670	0.28	0.28	0.28	24.7525	1
-2.950	0.29	0.29	0.29	20.4918	1
-3.240	0.30	0.3	0.3	16.9492	1
-3.540	0.32	0.32	0.32	13.8696	1
-3.860	0.34	0.34	0.34	11.0988	1
-4.200	0.36	0.36	0.36	8.3472	1
-4.560	0.38	0.38	0.38	3.951	1

-4.940	0.40	0.4	0.4	1	1
-5.340	0.42	0.42	0.42	1	1
-5.760	0.44	0.44	0.44	1	1
-6.200	0.47	0.47	0.47	1	1
-6.670	0.51	0.51	0.51	1	1
-7.180	0.55	0.55	0.55	1	1
-7.730	0.60	0.6	0.6	1	1
-8.330	0.66	0.66	0.66	1	1
-8.990	0.73	0.73	0.73	1.5931	1
-9.720	0.80	0.8	0.8	2.4963	1
-10.520	0.90	0.9	0.9	3.8197	1
-11.420	1	1.0	1.0	6.0569	1
-12.420	1.12	1.12	1.12	7.5529	1
-13.540	1.25	1.25	1.25	9.1912	1
-14.790	2.5	2.5	2.5	9.4787	1
-17.290	5	5.0	5.0	9.4787	1
-22.290	10	10.0	10.0	9.4787	1
-32.290	20	20.0	20.0	9.4787	1

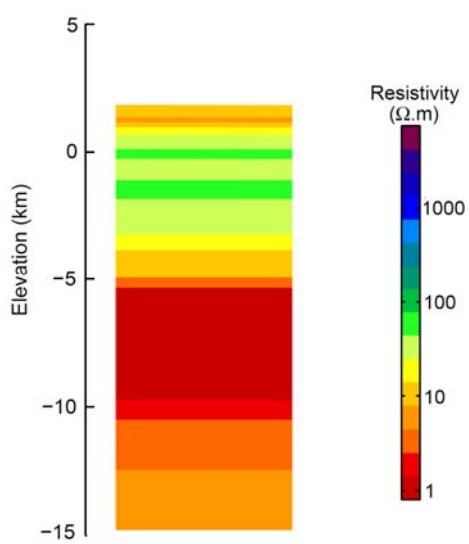

Figure 2.4.3: Graphic representation of the background resistivity layers.

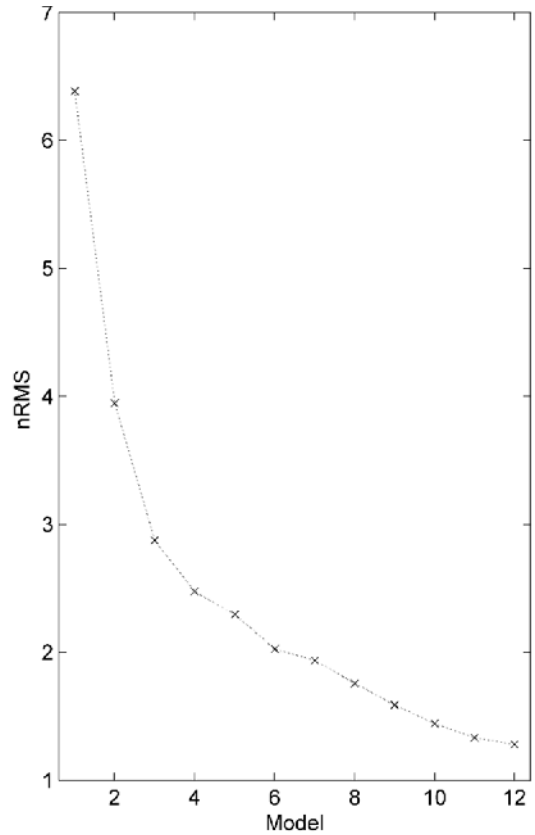

Figure 2.4.4. nRMS for each successive model generated by the inversion.

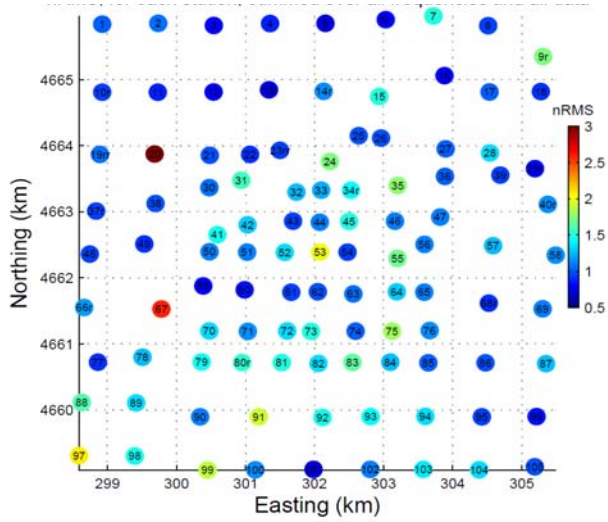

Figure 2.4.5. Distribution of the nRMS for individual MT stations.